中國造船暨輪機工程學刊第七卷第一期(民國七十七年)
Journal of the Society of Naval Architects and Marine Engineers, R.O.C., Vol. 7, No. 1, pp.17-24 (1988)

ON A NUMERICAL STUDY OF COMBUSTION PROCESS WITHIN A MARINE DIESEL ENGINE

Lee Shi-Min,* Tony W. H. Sheu**
* System engineer and Lecture Computer Education Center
Tamkang University
** Institute of Naval Architecture
National Taiwan University

Keywords: ICE-ALE scheme, combustion, Marine Diesel engine.

ABSTRACT

A numerical study on combustion processes within the RT Diesel engine is made. The cylindrical form of transient governing equations for chemical species within an internal combustion chamber are analyzed by a combined ICE-ALE finite difference scheme which is capable of handling the boundary surfaces of moving piston effectively. The compressed heated homogeneous flameable mixture is ignited before the end of compression stroke of compression ignition. The fuel injection occurring on compression ignition is not modelled for simplicity. The chemical processes include both kinetic reactions and partial equilibrium reactions. The computed contours of dependent variables, realistic pressure–volume diagram, and distributions of NO and CO may provide the picture of flowfield as well as a useful data–base for designers.

以數值計算方法模擬船用柴油引擎內的燃燒現象

李 世 鳴* 許 文 翰**
* 淡江大學電腦教學中心
** 國立台灣大學造船工程研究所

摘 要

本文嘗試以數值方法探討在 RT 柴油引擎內的燃燒現象。以ICE-ALE有限差分方法解析發生在隨時間變化的燃燒室的化學主導方程組。基于簡化計算的理由，在壓縮燃燒中的噴油模型暫不考慮。計算結果以各主要變數的等高線，P-V圖形，及 NO，CO 的質量分佈表示。此一流場模擬可以提供設計者有用的資料。

INTRODUCTION

The increasing demand in developing a numerical technique to predict the multi-component chemically reactive flowfield of practical importance has attracted several research groups around the world. The group led by C. W. Hirt at Los Alamos Scientific Research Laboratory has developed a CONCHAS [1] code under this consideration. This code, based on a series of SOLA methods [2], is used to analyse the transient solutions in terms of primary variables following a sequence of finite time

increments. The computed results by this code and certain spray model have been recognized to be successfully and widely used in the car industry.

Diesel engines are commonly found in trucks, buses, and marine main propulsion engines. The mechanical work for propelling the ship is converted from the release of chemical energy of injection fuel during the compression ignition (CI) combustion process. The fuel droplets are vaporized as it was sprayed into the combustion chamber which is full of compressed high temperature air. The combustion begins if the ignition temperature is reached. In two-stroke Diesel engine, it is usually equiped with scavenging blowers to assist the exhaust process.

CONCHAS utilizes a partially implicit numerical scheme, a variant of ICE method [3], to advance the transient solutions in a series of computation phases. The spatial difference scheme ALE [4] is operated on the integral form of governing equations. The vertices of the cell are allowed to proceed in an arbitrary Lagrangian–Eulerian manner which is suitable to represent curved or moving boundaries. Chemical reactions of kinetic and equilibrium types are incorporated into the formulation by representing the corresponding contribution in the source terms.

The analysis on actual combustion process is attempted in this study. The governing equations of integral forms for representing the physics of present interest are included in the next section. A brief description of major steps in numerical algorithm and some subsidiaries for solving these equations accurately are included. The flow configuration of the working problem and its corresponding computed results are made also. The prediction on exhaust gas turbocharging and air scavenging processes for completing the cycle analysis will be presented in the subsequent publications.

BASIC FORMULATION

The basic equations governing the flowfield is formulated over either two–dimensional Cartesian or cylindrical coordinate system. The primary variables are chosen to be partial mass density, pressure, velocity components at the vertices of regular cells, swirl velocity perpendicular to physical plane, and internal energy. The coupled system of continuity equation for species k, momentum equations, energy equation, swirl equation, and equations of state are used to describe the physics of the flowfield.

The conversion of above equations to the corresponding integral forms is required since the balance is performed over the control volume. The integral types of governing equations are:

Continuity equation for species k:

$$\frac{d}{dt}\int_A R\rho_k dA + \oint_p R\rho_k(\underline{u}-\underline{b})\cdot\underline{n}\,ds = \oint_p R\rho D\nabla\left(\frac{\rho_k}{\rho}\right)\cdot\underline{n}\,ds + \int_A R(\dot{\rho}_k)dA \qquad (1)$$

where $R = \chi^{\delta}$: $\delta = 0$ and $\delta = 1$ represent rectangular and cylindrical coordinates respectively. The subscript below the integral symbol, A and p, represent control area and its perimeter respectively. The chemical source term $\dot{\rho}_k$ is given by

$$\dot{\rho}_k = \mu_k \sum_r (b_{kr} - a_{kr})\,\dot{\omega}_r$$

for the chemical reaction system at r-th reaction.

$$\sum_k a_{kr}X_k \rightleftharpoons \sum_k b_{kr}X_k$$

The rate of progress of r-th reaction $\dot{\omega}_r$ for kinetic reaction is represented by

$$\dot{\omega}_r = k_{fr}\prod_k\left(\frac{\rho_k}{\mu_k}\right)^{a'_{kr}} - k_{br}\prod_k\left(\frac{\rho_k}{\mu_k}\right)^{b'_{kr}}$$

$$k_{fr} = A_{fr}\,T^{\xi_{fr}}\exp\left(-\frac{E^{+}_{fr}}{T}\right)$$

$$k_{br} = A_{br}\,T^{\xi_{br}}\exp\left(-\frac{E^{+}_{br}}{T}\right)$$

Overall continuity equation:

$$\frac{d}{dt}\int_A R\rho dA + \oint_p R\rho\,(\underline{u}-\underline{b})\cdot\underline{n}\,ds = 0 \qquad (2)$$

where $\rho = \sum_k \rho_k$ is the total density.

Momentum equations:

$$\frac{d}{dt}\int_A R\rho\underline{u}dA + \oint_p R\rho\underline{u}(\underline{u}-\underline{b})\cdot\underline{n}\,ds$$
$$= -\int_A R\underline{\nabla}P dA + \oint_p R\underline{\underline{\sigma}}\cdot\underline{n}ds + \int_A(\rho w^2-\sigma_0)\underline{\nabla}R dA$$
$$+\int_A R\rho\underline{G}dA \qquad (3)$$

The viscous two-dimensional and cylindrical stresses are given respectively by

$$\underline{\underline{\sigma}} = \mu[(\underline{\nabla}\underline{u}) + (\underline{\nabla}\underline{u})^T] + (\frac{\lambda}{R})\underline{\nabla}\cdot(R\underline{u})\underline{\underline{I}}$$
$$\sigma_0 = (-\frac{2\mu}{R})\underline{u}\cdot\underline{\nabla}R + (\frac{\lambda}{R})\underline{\nabla}\cdot(R\underline{u})$$

Swirl equation

$$\frac{d}{dt}\int_A R^2\rho w dA + \oint_p R^2\rho w(\underline{u}-\underline{b})\cdot\underline{n}\,ds$$
$$= \oint_p R\underline{\tau}\cdot\underline{n}\,ds \qquad (4)$$

where the swirl stress vector is given by

$$\underline{\tau} = \mu R^2\underline{\nabla}(\frac{w}{R})$$

Energy equation:

$$\frac{d}{dt}\int_A R\rho I dA + \oint_p R\rho I(\underline{u}-\underline{b})\cdot\underline{n}\,ds$$
$$= -\int_A p\underline{\nabla}(R\underline{u})dA + \int_A R\underline{\underline{\sigma}}:\underline{\nabla}\underline{u}dA$$
$$+\int_A R\underline{\tau}\cdot\underline{\nabla}(\frac{w}{R})dA + \int_A \sigma_0\,\underline{u}\cdot\underline{\nabla}R dA$$
$$-\int_p R\underline{J}\cdot\underline{n}ds + \int_A R\dot{Q}dA \qquad (5)$$

The heat flux vector $\underline{J}$ is given by

$$\underline{J} = -k\underline{\nabla}T - \rho D\sum_k h_k\underline{\nabla}(\frac{\rho_k}{\rho})$$

The chemical heat release is given by

$$\dot{Q} = \sum_r q_r\dot{w}_r$$

for kinetic reaction.

Equations of state:

$$p = R_g T\sum_k(\frac{\rho_k}{\mu_k})$$
$$I(T) = \sum_k(\frac{\rho_k}{\rho})I_k$$
$$C_v(T) = \sum_k(\frac{\rho_k}{\rho})C_{vk}$$
$$h_k(T) = I_k + \frac{R_g T}{\mu_k} \qquad (6)$$

Chemical reaction:

The chemical reactions,involving 12 species in the combustion process, include three kinetic reactions and six equilibrium reactions [1]. The kinetic reactions employed are:

$$2C_8H_{18} + 25\,O_2 \rightarrow 16\,CO^2 + 18H_2O$$
$$N+O_2 \rightleftharpoons NO + O$$
$$O+N_2 \rightleftharpoons NO + N$$

The equilibrium reactions are assumed to be

$$H_2 \rightleftharpoons 2H$$
$$O_2 \rightleftharpoons 2O$$
$$N_2 \rightleftharpoons 2N$$
$$2H_2O+O_2 \rightleftharpoons 4OH$$
$$O_2+2CO \rightleftharpoons 2CO_2$$
$$O_2+H_2 \rightleftharpoons 2OH$$

where the rate coefficients and equilibrium constants can be obtained from experiment measurements [5].

NUMERICAL ALGORITHM

The employed numerical technique combines the use of ICE method for time discretization and ALE method for spatial discretization. The temporal part of difference scheme is partially implicit such that the stability limitation generated by purely explicit scheme is removed. The spatial difference scheme is constructed by applying an integral–balance on the fluxes within an arbitrary quadrilaterals. The preservation of local conservation of properties is therefore expected.

The spatial region is spanned by a number of quadrilateral cells. The corners or vertices of the cell may move in an arbitrary prescribed manner such that the Lagrangian and Eulerian desctiptions turn out to be the special cases. The calculations are basically performed over two different types of grid, namely regular cell (i, j) in figure 1 and momentum cell (i,j) in figure 2. All primary variables but velocities are assumed to be uniform within the regular cell and on the cell surface. The momentum cell (i, j), centered about vertex (i, j), contains four triangular subcells of its neighboring regular cells. Velocities are regarded as uniform within each momentum cell. The values of velocity components are those at the vertex on which the momentum cell is centered.

The computed values of flow properties are not advanced directly within a time step. Those quantities are instead updated following a series of stages, namely explicit Lagrangian phase, pressure iteration phase, and rezone phase. The detailed procedures of formulation are described in reference [1], only a brief description is made below.

The dependent variables in phase 1 are updated in an explicit Lagrangian (b = u) manner without considering the contributions by convective terms. The intermediate values of partial cell density, total cell density, cell internal energy, pressure, momentum cell mass, vertex velocities, and swirl velocity are then evaluated.

The correction on velocity components due to the omission of pressure gradient terms in phase 1 is made in the pressure iteration step. The updated veloccities are calculated implicitly from the equations for x_{ij}, y_{ij}, u_{ij}, v_{ij} and p_{ij} by a pointwise iterative procedure.

The values of fluid properties are finally updated in rezone phase which accounts for the transport of chemical species, momentum, and energy due to the relative motion, $b \neq u$, between fluid and mesh. The rate at which cell volume changes is incorporated to advance the solutions for primary variables to (n+1) time level.

The combined ICE-ALE difference scheme suffers a lack of communication between adjacent vertices in certain cases which may cause a slight oscillations in the velocity field. The node coupler technique is introduced to alleviate this problem by introducing a small amount of restoring acceleration at each vertex.

STABILITY CONSIDERATION

The stability restrictions due to the spatial difference in explicit Lagrangian phase are noted. Those numerical oscillations are introduced by diffusive processes of viscosity in momentum equations, thermal conductity in energy equation, and species diffusivity in species continuity equation. The overall diffusive stability condition is therefore chosen to be

$$\Delta t < \frac{A^2}{2\ell^2}\left[\max\left(\frac{4\mu}{3\rho}, \frac{k}{\rho C_v}, D\right)\right]^{-1}$$

where A and ℓ are cell area and maximum cell diagonal.

The stability restriction, introduced by spatial difference on convection terms in rezone phase within a rectangular mesh, is approximately by

$$\Delta t < \min\left[\frac{\Delta x}{(u-b_x)}, \frac{\Delta y}{(v-b_y)}\right]$$

NUMERTICAL RESULT

The single-acting two-stroke Sulzer RTA76 Diesel engine is used in the present study as a test problem. The ignition points or locations of fuel injectors are located symmetrically on the top of combustion chamber, Figure 3, such that the complex three-dimensional phenomena can be avoided. The bore and stroke are 760 mm and 2200 mm respectively. The temperature of air within the cylinder is maintained at 42°C initially with kinematic viscosity 4.1 $(mm)^2/sec$. The temperature on the cylinder boundary is kept at 23°C by the surrounding

auxiliary cooling system. The ignition starts at 14.1 degree before the piston moves up to T.D.C. with 95 r.p.m. crank revolution speed.

The combustion starts, controlled by precise timing, in the viscinity of injector locations when the piston moves up to a specific location. At this moment the enclosed compressed air occupies a smaller volume than that at starting-injection for accounting for the ignition delay. The revolution of flame front propagation throughout the cylinder from the very beginning of localized ignition is developed. The corresponding velocity plot, contours of pressure, temperature, and density within the cylinder for every 100 time cycles are illustrated in Figures 8, 6, 7, 5 respectively. The mass concentrations of combustion products such as NO and CO are also plotted in Figure 9 and 10. As far as the distinction between the present actual combustion process and ideal air-standard Diesel cycle is concerned, a p-V diagram is prepared in Figure 4 where p is cell-averaged pressure.

The combustion process is not continuous but occurs cyclically. The order-of-time for completing the combustion process takes 10^{-3} second. The C.P.U. time for 100 time cycles is estimated approximately 180 seconds of PRIME 9955 II which is equivalent to VAX 8600.

CONCLUSION

A numerical prediction on combustion process during the compression stroke is made. The present study demonstrates the employed ICE-ALE difference scheme works fairly well for analysing chemical reaction from the practical point of view. The accuracy can be further improved if more mesh points are used, more detailed reaction steps, and precise liquid spray model are available.

NOMENCLATURE

R	x^{δ}
ρ_k	partial mass density.
ρ	total mass density
D	species diffusivity
$\dot{\rho}_k$	rate of change of ρ_k due to possible chemical reaction.
u	velocity vector at vertices of regular cell
b	bound velocity vector
σ	two-dimensional viscous stress tensor
σ_0	cylindrical viscous stress
G	external force per unit mass
W	swirl velocity
μ	first viscosity coefficient
λ	second viscosity coefficient
τ	swirl stress vector
E	internal energy
I	specific internal energy
J	heat flux vector
Q	rate of chemical heat release
k	thermal conductivity
Tq	temperature
h_k	partial specific enthalpy of species k
I_k	partial specific internal energy of species k
c_v	specific heat at constant volume
R_g	universal gas constant
μ_k	molecular weight of species k
$\dot{\omega}_r$	rate of progress of r-th reaction
a_{kr} b_{kr}	stoichimetric coefficients for the r-th reaction
X_k	one mole of species k
t	time
n	outward unit normal to perimeter p
I	two-dimensional unit dyadic
E_{fr}^{+}, E_{br}^{+}	Activation temperatures
k_{fr}, k_{br}	rate coefficients for reaction
x, y	physical coordinates

Subscript

f_r	forward reaction
b_r	backward reaction
k	

Superscript

T	transpose

REFERENCES

[1] T.D. Butler, L.D. Cloutman, J.K. Dukowicz, J.D. Ramshaw, CONCHAS, Los Alamos Scientific Laboratory, LA-8129-MS.

[2] C.W. Hirt, B.D. Nichols, and N.C. Romero, SOLA – A numerical solution algorithm for transient fluid flows, Los Alamos Scientific Laboratoary report LA-5852, 1975.

[3] F.H. Harlow and A.A. Ameden, Numerical calculation of almost incompressible flow, J. Comp. Phys. 3, 80, 1968.

[4] C.W. Hirt, A.A. Amsden, and J.L. Cook, An arbitrary Lagrangian-Eulerian computing method for all speeds, J. Comp. Phys. 14, 227, 1974.

[5] C. Olikara, and G.L. Borman, A Computer program for calculating properties of equilibrium combustion products with some applications to I.C. engines, SAE paper No. 750468, 1975.

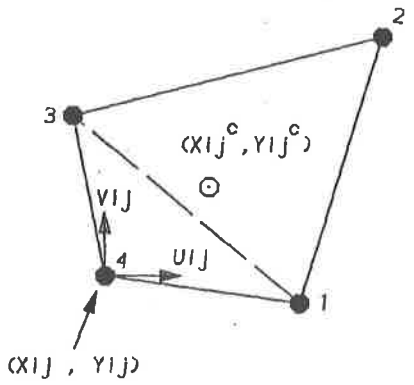

Fig. 1 Typical finite difference cell. The velocity components are stored at points ● ; The other flow properties are stored at cell center ⊙

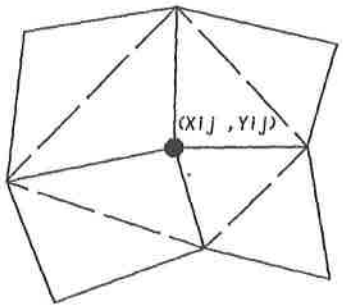

Fig. 2 Momentum cell is represented by the dashed line where point ● is the common vertex of four adjacent regular cell.

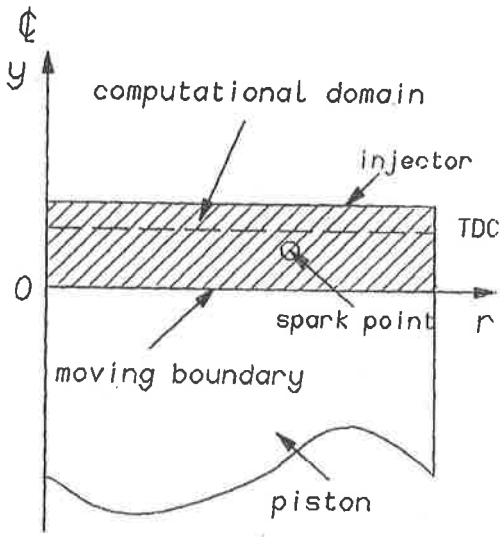

Fig. 3 Configuration for computational domain.

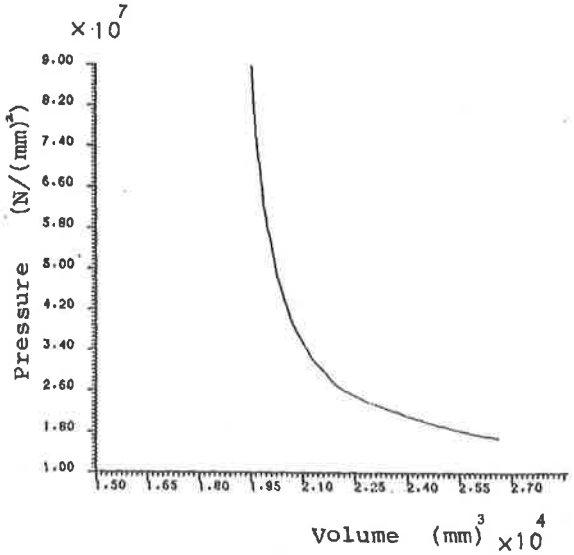

Fig. 4 A P-V diagram for the combustion process where the pressure is averaged over the corresponding volume of the chamber.

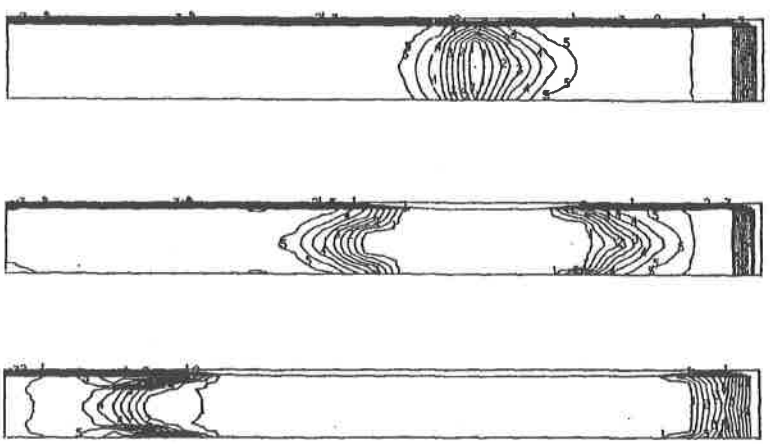

Fig. 5 The density contour within the combusion chamber. The contour plots from above to bottom indicate the densities at time $t=0.164\times10^{-3}$ sec, 0.317×10^{-2} sec, and 0.393×10^{-2} sec respectively.

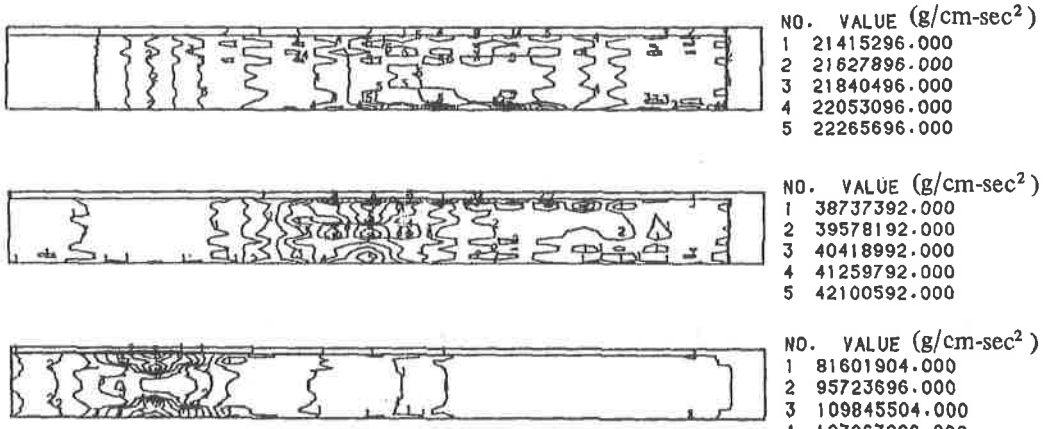

Fig. 6 The pressure contour within the combustion chamber. The contour plots from above to bottom indicate the pressures at time $t=0.164\times10^{-3}$ sec, 0.317×10^{-2} sec, and 0.393×10^{-2} sec respectively.

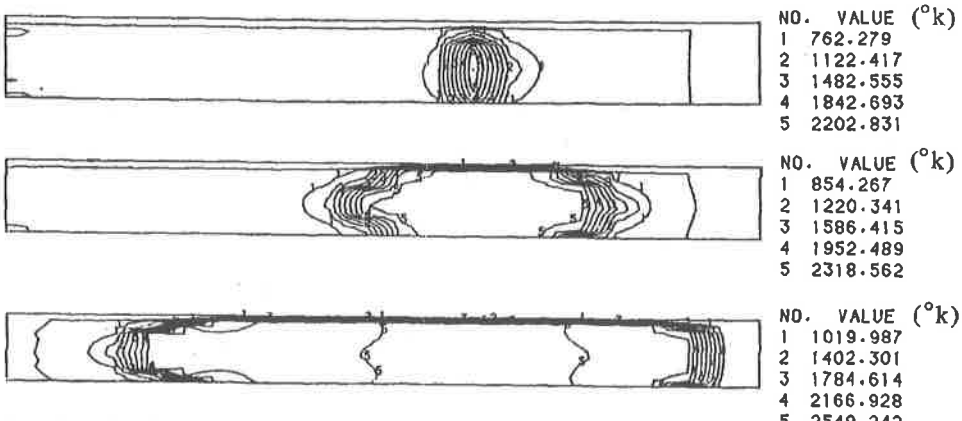

Fig. 7 The temperature contour within the combustion chamber. The contour plots from above to bottom indicate the temperatures at time $t=0.164\times10^{-3}$ sec, 0.317×10^{-2} sec, 0.393×10^{-2} sec respectively.

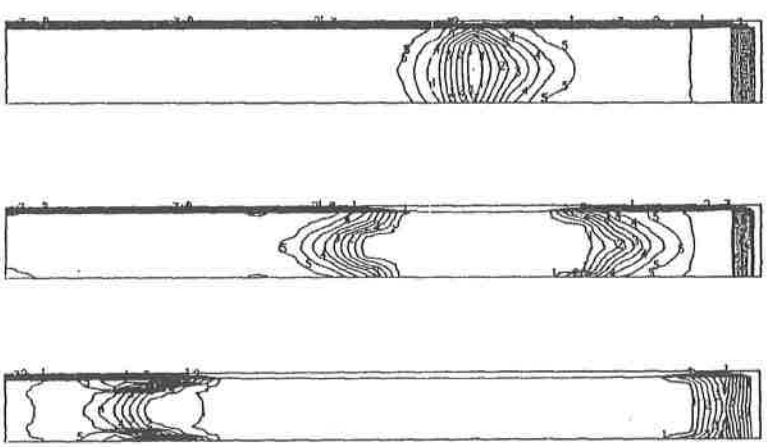

Fig. 5 The density contour within the combusion chamber. The contour plots from above to bottom indicate the densities at time $t=0.164\times10^{-3}$ sec, 0.317×10^{-2} sec, and 0.393×10^{-2} sec respectively.

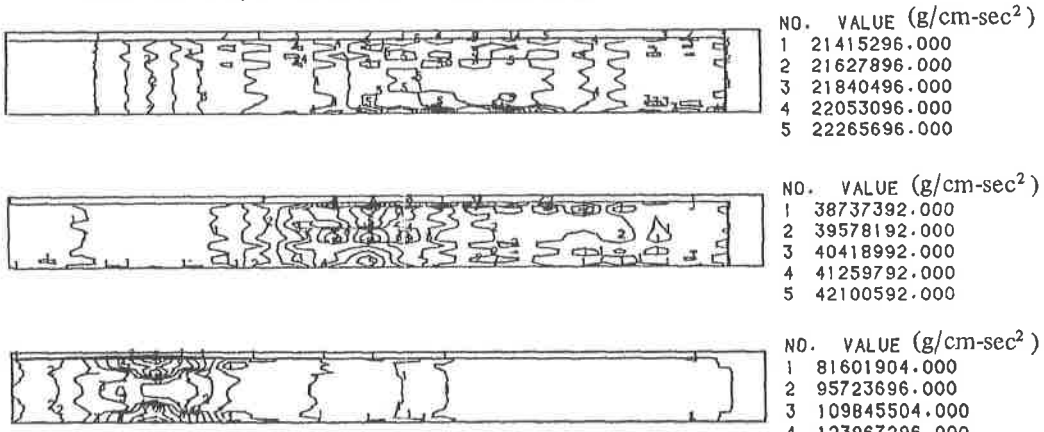

Fig. 6 The pressure contour within the combustion chamber. The contour plots from above to bottom indicate the pressures at time $t=0.164\times10^{-3}$ sec, 0.317×10^{-2} sec, and 0.393×10^{-2} sec respectively.

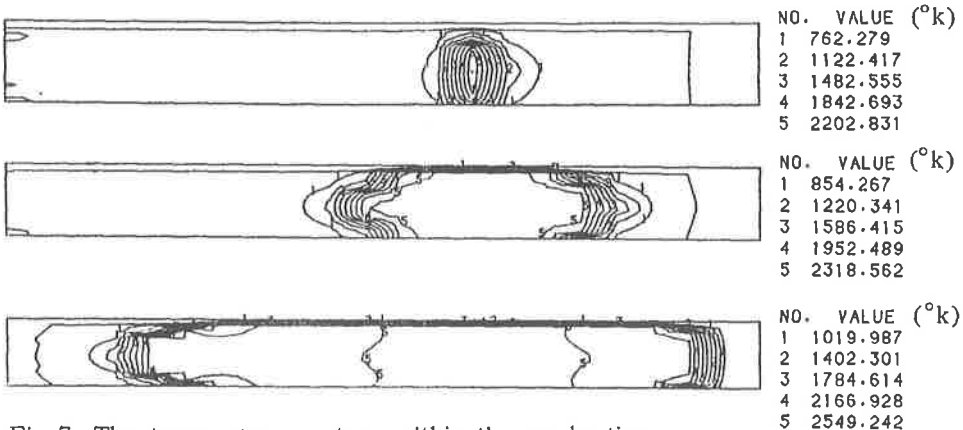

Fig. 7 The temperature contour within the combustion chamber. The contour plots from above to bottom indicate the temperatures at time $t=0.164\times10^{-3}$ sec, 0.317×10^{-2} sec, 0.393×10^{-2} sec respectively.

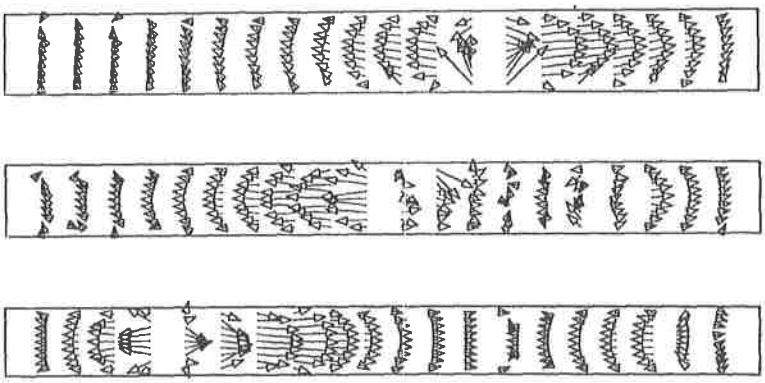

Fig. 8 The velocity vector plot. The contour plots from above to bottom indicate the velocity vectors at time $t=0.164\times10^{-3}$ sec, 0.317×10^{-2} sec, and 0.393×10^{-2} sec respectively.

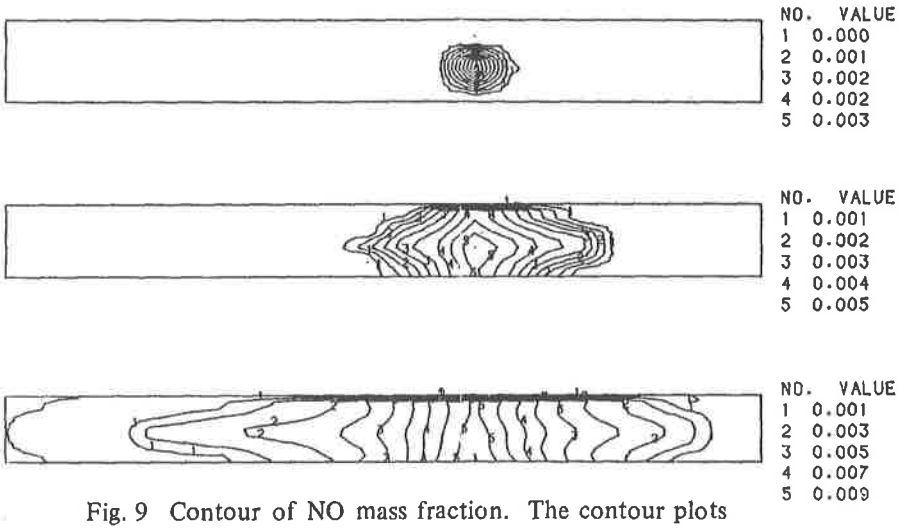

Fig. 9 Contour of NO mass fraction. The contour plots from above to bottom indicate the NO mass fractions at time $t=0.164\times10^{-3}$ sec, 0.317×10^{-2} sec, and 0.393×10^{-2} sec respectively.

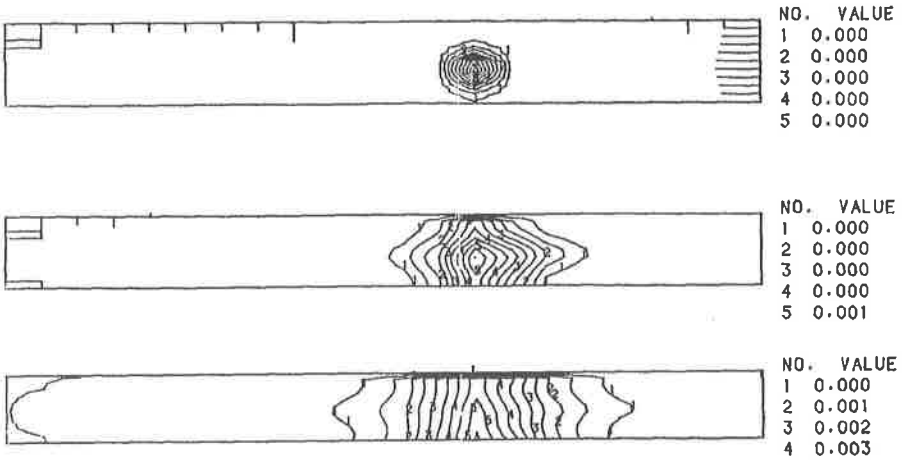

Fig.10 Contour of CO mass fraction. The contour plots from above to bottom indicate the CO mass fraction at time $t=0.164\times10^{-3}$ sec, 0.317×10^{-2} sec, and 0.393×10^{-2} sec respectively.